11th World Congress on Computational Mechanics (WCCM XI)
5th European Conference on Computational Mechanics (ECCM V)
6th European Conference on Computational Fluid Dynamics (ECFD VI)
E. Oñate, J. Oliver and A. Huerta (Eds)

NUMERICAL SIMULATION OF THE INFLUENCE ON INTERSTITIAL FLUID FLOW AND ION TRANSPORT OF THE VISCOUS MECHANICAL BEHAVIOR OF HUMAN SKIN IN VIVO

M-A. ABELLAN[*], J-M. BERGHEAU[*] AND H. ZAHOUANI[*]

Université de Lyon, ENISE, LTDS, UMR 5513 CNRS,
58 rue Jean Parot, 42023 Saint-Etienne Cedex 2, France.
e-mail: marie-angele.abellan@enise.fr
e-mail: jean-michel.bergheau@enise.fr
e-mail: hassan.zahouani@ec-lyon.fr

Key Words: *Porous media, Human skin, Numerical simulation, Fluid and ion transport, Viscoelastic material, Indentation test.*

Abstract. This paper proposes a tri-phasic model of human skin. The skin is seen here as a deforming stratified medium composed of three layers and made out of different fluid-saturated materials which contain also an ionic component. In each layer, the interstitial fluid is treated as a Newtonian viscous fluid described by its own behavior law while the linear isotropic behavior of the solid is investigated with first an elastic law and then with a Kelvin-Voigt viscoelastic law. The numerical simulations of in vivo indentation test performed on human skin in vivo allows for a quantitative understanding of fluid flows and ion transport influenced by the deformations of the skin layers soft tissues.

1 INTRODUCTION

The human skin is the external protection of the human body. It protects the body against external chemical, biological, mechanical and thermal influences. From the skin outer surface inward, it is composed of several layers: the epidermis (consisting of the stratum corneum and the viable epidermis), the dermis and the hypodermis. Each layer has a unique structure and function contributing to the in vivo overall material function of the human skin. Studying the answers of these skin layers is important for clinical and cosmetic researches, such as the development of personal care products, the understanding of skin diseases and the consequences of chirurgical or medical actions.

Numerous studies have shown that the skin is a stratified non-homogeneous, anisotropic, non-linear viscoelastic material which is subjected to a pre-stress in vivo. In addition its properties vary with age, throughout the body and depending on the health of the person. The properties are also influenced by the structure of each layer, where the cells of the soft tissues are bathed and hydrated by an interstitial tissue fluid which provides them with nutrients and which removes their wastes. The composition of interstitial fluid depends upon the exchanges between the cells in the skin layers, the blood and the lymph circulations. The plasma, interstitial fluid and lymph compartments are linked and fluid flows continuously from one compartment to the next [1]. This means that interstitial fluid as a different composition in

different tissues and areas of the body. Since the work of Starling on fluid filtration [2], researches have shown that exchange microvasculature is a dynamic, multi-cellular structure subject to adaptation to stimuli [3, 4, 5, 6]. These regulatory mechanisms influence the routes governing solute and water transport by and across blood micro-vessels and lymphatic micro-vessels and their contribution to tissue homeostasis [7]. Moreover, it is thought that the directions of movement of water and solute are also influenced by gradients of both hydrostatic and oncotic pressures across the microvasculature walls. As a direct consequence, these phenomena are complex to understand and to model due to the strong couplings that exist between them and due to the complex behavior of the different soft tissues of skin.

Over the past decades there has been a tremendous development in techniques aiming to characterize the mechanical behavior of human skin and to overcome inherent difficulties associated with measuring the tribological properties of skin in vivo without too much modifying the skin's natural state of stress. The experimental set-up considered here as support for characterizing in vivo equivalent parameters of human skin without pre-stressing the skin before the test is the LTDS-light load indentation device.

The sophistication of theoretical and computational models of skin biomechanics has increased and addressed the challenge to include the measured mechanical characteristics into computer models to simulate the non-linear anisotropic behavior of skin. Among them, a quasi-linear viscoelastic model is proposed in [8] for pig skin samples and in [9] to simulate the deformation of in vivo facial skin. Again for facial animation, reference [10] uses a plastic-viscoelastic model with a Maxwell dashpot to simulate wrinkle generation depending on the whole history of facial animation. Within the framework of a general phenomenological thermo-hydro-mechanical and physico-chemical approach of heterogeneous media [11], a tri-phasic skin model is proposed in reference [12] and applied in [13] for a solid phase with four solid materials, a fluid phase with four fluid materials and ions under ambient constant conditions with no electrical effects. In this model, skin is seen as a stratified material with four layers modelling the four outer layers of skin: the stratum corneum, the viable epidermis, the dermis and the hypodermis. These four layers are modelled separately in order to win insights on their own contribution to the overall response of the skin. All layers are supposed to be made of fluid-saturated materials. Furthermore each layer is a different solid material within the solid phase and it is described by its own linear elastic behavior law. In the fluid phase, the four fluids model the interstitial fluid of each skin layer of soft tissue seen as a Newtonian viscous fluid described by its own behavior law.

This paper proposes an extension of this skin model. Now the solid materials are seen as linear viscoelastic materials, each of them with its own behavior law.

To provide a proper setting, we will first present the context of this paper linked to the histology of human skin in vivo and the consequences on the skin model. Then the governing equations for a deforming tri-phasic medium are recapitulated before presenting briefly the non-invasive experimental device. Example calculations are done with a finite difference analysis coupled with an iterative procedure for a specimen of skin. The obtained numerical results are discussed. Finally, some concluding remarks are made.

2 HYSTOLOGY OF SKIN

Skin has a stratified structure consisting of four main layers (which are from the surface

inward: stratum corneum, viable epidermis, dermis and hypodermis) plus the circulatory system (including the blood and lymphatic systems) plus loose connective tissues and the interstitial fluid (that fills the space located between the capillary walls and the cells and/or between the cells) (Fig. 1). These layers are attached to (and separated from) each other by thin layers of extracellular matrix proteins called the basement membrane [14]. A detailed look to these different layers shows up the following points:

- The hypodermis is the adipose tissue found between the dermis and the muscles. It can be some millimetres thick depending on the anatomical site on the body, on the age, the sex, the race and the health of the person.This adipose tissue is a loose association of white adipocytes held in a framework of collagen fibres. Lipid is the predominant component of the adipocytes which act as storage cells for the body. The lipid droplet can sometimes exceed 50 μm. Adipose tissue has little extracellular matrix compared to other connective tissues. It is mainly an insulating layer and a protective cushion.
- The dermis is usually a 1 to 4 mm thick layer. It contains microstructures like blood vessels, lymph vessels, nerve endings, sweat glands, sebaceous glands and hair follicles. Scattered throughout the dermis are cells called fibroblasts which regulate the organisation of the fibrillar dermal matrix. Apart from that the dermis is a very dense network of collagen type I fibres and elastin fibres with minute quantities of reticulin within a significant amount of amorphous ground substance, all bathed in interstitial fluid. The amorphous ground substance or extrafibrillar matrix is primarily composed of glycosaminoglycans which are highly polar and attract water. This ability makes the amorphous ground substance able to combine with the water of the interstitial fluid to form a viscous gel-like material, which does not leak out of the dermis, even under high pressure. This viscous gel combined with the fibrous network contributes to the protection of vessels and cells against mechanical insults. It is though that the collagen provides strength, the elastin maintains the elasticity of the tissue and the gel-like substance acts as a lubricant for the body or as a shock absorber.
- The viable epidermis consists of multi-layered polarized epithelium of viable keratinocytes, 10-100 μm thick. In the basal layer which contacts the basement membrane laying between the dermis and the viable epidermis, the cells continually divide during the lifetime of the organism, providing a source of cells which progressively migrate upwards through the layer, differentiating and stratifying to become hexagonal flat non-viable corneocytes. The viable epidermis is a non-vascular structure which also contains melanocytes, Langerhans cells and Merkel cells. Cells are surrounded, nourished and bathed by the interstitial fluid originating in the underlying dermis and transported across the epidermal-dermal junction. The cells are tied together by very strong desmosomes bridges providing resistance to shearing forces in this compact tissue. The intercellular spaces occupy less than 2% of the volume.
- The stratum corneum is a 10-25 μm thick layer composed of corneocytes held together by lipid bridges and corneosomes in what is commonly referred to as a brick-and-mortar structure. The intercellular spaces are about 0.1-0.3 μm and only 10% bounded water is found in the lipid mortar. Because of its structure and composition, the stratum corneum acts as a protective barrier. The stratum corneum and the viable epidermis are continuously renewed by desquamation within 6 to 30 days.

- The interstitial fluid is a tissue fluid i.e. a solution that bathes and surrounds the cells of soft skin tissues. It provides nourishment and waste removal for the cells, as well as transport of immune cells. It is the main component of the extracellular fluid, which also includes plasma and trans-cellular fluid. The amount of interstitium is about 50% of wet weight in skin. On average, a person has about 11 litres of interstitial fluid. Interstitial fluid consists of a water solvent containing sugars, salts, fatty acids, amino acids, coenzymes, hormones, neurotransmitters, oxygen, as well as waste products from the cells. The interstitial fluid is an ultra-filtrate of plasma with a total protein concentration of 50-60% of that in plasma and with an electrolyte composition similar to that of plasma. Moreover the composition of interstitial fluid depends upon the exchanges between the cells in the skin layers, the blood and the lymphatic vessels. The composition of the interstitial fluid with respect to proteins in plasma is a function of the fluid flux across the capillary, the size and charge of the molecule in question, as well as the barrier properties of the capillary wall. This leads to interstitial fluid with a different composition in the different layers of skin soft tissues. The interstitial fluid volume is normally kept within tight boundaries by automatic re-adjustments of the trans-capillary fluid flux when the capillary filtration is increased or decreased.

3 CONSEQUENCES ON THE SKIN MODEL

Skin soft tissues appear to be made out of several non-linear anisotropic hyper-elastic and viscoelastic solid materials and several compressible Newtonian viscous interstitial fluid components. For the specimen of human skin soft tissues studied here (Fig. 2) the choice is made to see the skin as a stratified tri-phasic material with:

- four layers: layer 1 simulates the stratum corneum, layer 2 accounts for the viable epidermis, layer 3 simulates the dermis, layer 4 is for the hypodermis;
- four solids in the solid phase: solid 1 simulates the corneocites and the lipid mortar present in the stratum corneum, solid 2 simulates the evolving cells of the viable epidermis, solid 3 simulates the different cells of the dermis including the lymph and blood vessels, solid 4 simulates the fatty connective tissue of the hypodermis;
- four fluids in the fluid phase: fluid 1 simulates the 10% bound water in the lipid mortar of the stratum corneum, fluid 2 for the interstitial fluid in the viable epidermis, fluid 3 for the interstitial fluid in the dermis, fluid 4 for the interstitial fluid in the hypodermis;
- ions simulating some cream deposited on the stratum corneum either for aesthetic or medical purposes and of which it is relevant to follow the penetration path and time.

Hence for each layer, the skin specimen simplifies to a solid, a fluid and the ions.

4 THEORETICAL MODEL

The phenomenological THMPC approach of heterogeneous media [11] gives a good framework for deriving the skin model detailed here after under the following assumptions: the behavior of each individual component depends on the behavior of all the other components present in the specimen of human skin, each individual component contributes to the overall response of the skin specimen in the percentage of its volumic ratio, a finite number of components are present in an infinitesimal volume of the skin specimen, all the components are extended to the total studied unit volume of the skin specimen, the reference

domain coincides with the initial configuration of the skin solid skeleton. The subscript π=s will be used for the solid, π= f for the fluid and π=i for the ions. The field equations are derived under the hypothesis of small displacement gradients, inert constituents (no mass transfer and no chemical reactions between the constituents), intrinsically incompressible constituents (the absolute mass densities are constant), electrical effects not taken into account, temperature is constant all along the study. The source of mass of constituent π coming from the other constituents present in the medium is equal to zero for inert constituents. Hence the balance of mass for each constituent π simplifies to:

$$\frac{\partial}{\partial t}\rho_\pi + \nabla.[\rho_\pi\, v_\pi] = 0 \qquad \text{(for } \pi\text{=s, f, i)} \tag{1}$$

with v_π absolute velocity of constituent π, ρ_π relative mass density of constituent π defined by $\rho_\pi = n_\pi\, \rho'_\pi$ (for π=s, f, i) where n_π is the volumic ratio of constituent π and ρ'_π is the absolute mass density of constituent π. Further, the sum of volumic ratios over the constituents present in the medium should equal one. Neglecting inertia forces, convective terms and the gravity acceleration, the balance of linear momentum for each constituent π reduces to:

$$\nabla.\sigma_\pi + p'_\pi = 0 \qquad \text{(for } \pi\text{=s, f, i)} \tag{2}$$

with σ_π the Cauchy stress tensor of constituent π, p'_π the source of momentum for constituent π coming from the other constituents. As this source term takes into account the possible local drag interactions between the solids, the fluids and the ions, their sum over the constituents present in the medium should equal zero. Then the material relations encompass the way solid, fluid and ions interact together. The chemical potential for the fluid reads:

$$\mu_f = p_f - \Pi_f + \psi_f = \left(\left(e^{(9.7).10^{-5}}\right) - e^{\frac{(9.7).10^{-5}}{n_f}}\right)(9.84).10^{10} + 3\,R\,T\,c_i \tag{3}$$

with p_f the pressure of fluid f, ψ_f the matrix potential for fluid f accounting for fluid-solid interactions (capillary and adsorptive effects), Π_f the osmotic pressure for fluid f accounting for fluid-ions interactions, R the universal gas constant, T the absolute temperature, c_i the concentration of the ions per unit fluid volume. For the ionic component, the chemical potential μ_i is defined as

$$\mu_i = \mu_{i0} + RT\ln(c_i) \tag{4}$$

with μ_{i0} chemical potential of the ions in a reference state. The generalized Darcy's law expresses fluid flow through a saturated porous medium in presence of an ionic component. When neglecting couplings between velocity and heat flux, it reads:

$$n_f(v_f - v_s) = -K_f\left[\nabla\mu_f + \frac{n_i}{n_f}\nabla\mu_i\right] \tag{5}$$

with K_π the permeability coefficient. The diffusion of ions through the fluid phase of a porous medium is taken into account through a Fick's law-type relation in which the velocity of the ions is governed by the velocity of the interstitial fluid filling the interstitial space of the skin layer through which the ions are transported and is expressed by:

$$n_i(v_i - v_f) = -D_i\ \nabla\mu_i \tag{6}$$

with D_i the diffusion coefficient of the ions. In the following, the constitutive relations are elaborated under the classical assumption for heterogeneous media that the total Cauchy stress tensor is composed of a solid and a fluid part

$$\sigma = \sigma_s + \sigma_f + \sigma_i \tag{7}$$

with σ the total Cauchy stress tensor. The Newton viscous stress-velocity relation for the fluid expresses the Cauchy stress tensor of the fluid σ_f as

$$\sigma_f = -\,p_f\, I + 2\,\widetilde{\mu_f}\,\nabla\, v_f + \widetilde{\eta_f}\,\left(\nabla \cdot v_f\right) I \tag{8}$$

where $\widetilde{\mu_f}$ is the dynamic viscosity of the fluid, $\widetilde{\eta_f} = -\frac{2}{3}\,\widetilde{\mu_f}$ is the viscosity coefficient of the fluid. The stress relation for the ions assumes the Cauchy stress tensor of the ions to model a static isotropic stress state that would exists if the ions were at rest and which is defined as

$$\sigma_i = -\,p_i\, I \tag{9}$$

where p_i is the pressure of the ions. The stress-strain relation for the solid is investigated following two scenarios under the assumption of small displacements and strains.

Scenario 1: Skin is considered as a linear isotropic elastic material and a Hooke's stress-strain relation is taken for the solid

$$\sigma_s = D_s^e : \varepsilon_s \tag{10}$$

with D_s^e the elasticity tensor of the solid, $\varepsilon_s = \nabla^s u_s$ the strain tensor of the solid, u_π the displacement field of the solid. The superscript s denotes the symmetric part of the gradient operator.

Scenario 2: Skin is considered as a linear isotropic Kelvin-Voigt viscoelastic material. It is a two parameters system consisting of:

- a Hookean spring (modulus E_{Ks}) accounting for the purely elastic part of the behavior of the solid where stress $\sigma_{spring} = E_{Ks}\,\varepsilon_{spring}$ is proportional to strain ε_{spring}.
- and a Newtonian dashpot (viscosity η_s) representing the purely viscous part of the behavior of the solid where the stress $\sigma_{dashpot} = \eta_s\,\frac{\partial \varepsilon_{dashpot}}{\partial t}$ is proportional to the rate of deformation $\frac{\partial \varepsilon_{dashpot}}{\partial t}$ with time.

According to this model when a load is applied, both spring and dashpot start to shorten and if the load is removed they try to come back to their original position. In this configuration, the stress tensor of the solid σ_s is the sum of the stress of the spring and of the stress of the dashpot while the strain tensor of the solid ε_s equals the deformation of the spring which also equals the deformation of the dashpot. Stress and strain are then defined as

$$\begin{aligned} \sigma_s &= \sigma_{spring} + \sigma_{dashpot} = E_{Ks}\,\varepsilon_{spring} + \eta_s\,\frac{\partial \varepsilon_{dashpot}}{\partial t} \\ \varepsilon_s &= \varepsilon_{spring} = \varepsilon_{dashpot} \end{aligned} \tag{15}$$

5 EXPERIMENTAL DEVICE

Knowledge about the mechanical response of the human skin in vivo can be studied using the original LTDS-indentation device developed by the team of Prof. H. Zahouani. This light-load indenter is fixed to a rigid arm able to move with respect to a fixed rigid heavy support

(Fig. 2). As it is not necessary tying the indenter to the skin during the experiments, it does not disturb its natural stress state before application of the mechanical load. During an experiment, the indenter is manually positioned near the skin outer surface. Then the indentation device loads the skin mechanically by applying a controlled normal force onto the skin surface. The penetration depth of the rigid spherical indenter (diameter 6 mm) is recorded as a function of the normal applied force, Fload, during loading-unloading experiments. The recorded curve for an indentation test performed on the volar forearm of a volunteered young healthy adult is given in figure 3. The chosen location makes the indentation tests less tiring for the volunteer because of the position of the arm resting on a support all along the test, This location is easily accessible, relatively flat and in this position less disturbed by the natural movement of the body. Therefore it disturbs the less possible the skin's natural state of stress and consequently the recorded data. The indentation test is realized for a constant indentation speed of 500.0μm/s at ambient temperature and without surface treatment on skin before the test. For later use as loading-unloading steps of the numerical simulations, this recorded experimental curve (Fig. 3) is reworked and gives a curve of the applied mechanical load versus time (Fig. 3). Physically admissible boundary and initial conditions are also deduced from these experimental data and used in the numerical simulation.

6 NUMERICAL SIMULATION

6.1 Finite difference model

A finite difference analysis is carried out and the field equations described in section 4 are reworked for all the 9 constituents (for the four solids, the four fluids and the ionic component) present in the skin specimen given in section 2. The spatial derivatives appearing in the field equations and the material relations are approximated with a second-order accurate finite difference scheme. Explicit forward finite differences are used to approximate the temporal derivatives, which are first-order accurate. The fundamental unknowns are the velocity of the solid, the volumic ratio of the fluid and the concentration of the ions. The displacements are obtained by integration when needed. The incremental material relations give directly the increment of their associated variable. All calculations are done with the program THMPC for a specimen of skin of depth 1516 μm (12μm stratum corneum + 102μm viable epidermis + 1002μm dermis + 400μm hypodermis) and 380 elements (Fig. 1). The model is complemented by a set of material parameters taken as mean values for human skin available in the literature except as regards of the mechanical parameters for which a mechanical parameters estimation procedure is carried out in sub-section 6.2.

6.2 Mechanical parameters estimation procedure

The 12 mechanical parameters of the constitutive models of the two analysis are estimated by fitting the loading branch of the experimental load-displacement curve (Fig. 3) by an iterative procedure. They need to be estimated for respectively the stratum corneum (SC), the viable epidermis (VE), the dermis (DE) and the hypodermis (HY):

- For analysis1: 4 Young moduli E_{SC}, E_{VE}, E_{DE} and E_{HY}.
- For analysis 2: 4 Young moduli E_{KSC}, E_{KVE}, E_{KDE}, E_{KHY} and 4 viscosities η_{SC}, η_{VE}, η_{DE}, η_{HY}.

Material parameters are set in the input file of the finite difference model with the applied

load of the loading branch (Fig. 3). Then the simulation runs and the computed skin surface displacements during the loading steps are extracted and compared with the experimentally recorded axial displacement of the skin surface under the indenter. At the end of the procedure, the estimated mechanical parameters are:

- Analysis1: E_{SC} = 29E5 Pa, E_{VE} = 12E2 Pa, E_{DE} = 4E3 Pa, E_{HY} = 2E3 Pa ;
- Analysis 2: E_{KSC} = 46E5 Pa, E_{KVE} = 18.8E2 Pa, E_{KDE} = 6E3 Pa, E_{KHY} = 2E3 Pa and η_{SC} = 8E2 Pa, η_{VE} = 6E2 Pa, η_{DE} = 4E2 Pa, η_{HY} = 2E2 Pa.

Then the obtained values are used to calculate the unloading branch. Figure 6 shows the comparison between the experimental and the numerically obtained surface displacements curves for analysis 1 (Hooke) and analysis 2 (Kelvin-Voigt). Taking into account the low hysteresis exhibited by the experimental loading-unloading curve, the analysis 1 with elastic solid materials for describing the skin layers soft tissues were already giving a reasonably good fit. For analysis 2 and viscoelastic materials for describing the skin layers soft tissues, the obtained numerical results reproduce quite well the curve and maximum indentation depth of the experimental data. Figure 6 shows that the unloading curve is in good agreement with the experimental data with curves that are almost overlapping each other.

6.3 Numerical model

Therefore the computation is conducted for analysis 1 and analysis 2 with: the sets of mechanical parameters estimated in sub-section 6.2 for the skin soft tissues; an absolute mass density ρ'_s = 1330 kg.m^{-3} for the solids. The dynamic viscosities are taken equal to $\widetilde{\mu_{f1}}$ = 1.002E-3 Pa.s, $\widetilde{\mu_{f2}}$ =2E-3 Pa.s, $\widetilde{\mu_{f3}}$ =3E-3 Pa.s and $\widetilde{\mu_{f4}}$ =3.5E-3 Pa.s. An absolute mass density ρ'_f = 1000 kg.m-3 for the four interstitial fluids and an absolute mass density ρ'_i =1549 kg.m-3 for the ions. In the calculations, the permeability K= 1.98E-21 m^4.N^{-1}.s^{-1} and the diffusion coefficient D_i=3.3E-11 m^2.s^{-1} are adopted. Environmental conditions are assumed according to the following pattern (Fig. 2). For the upper skin surface: a force is applied at the upper node equivalent to the imposed loading steps (Fig. 6), atmospheric pressure for the fluid, the skin surface is in contact with a 0.15 [M] NaCl solution. For the inward skin surface: the lower node is subjected to a displacement condition of 0 mm displacement, a zero flux of fluid and a zero flux of ions. In the initial state, all layers are considered made out of fully saturated material with no ionic component. Moreover with respect to the volumic ratio of the ions, it is set equal to zero for all the layers in the initial state.

6 RESULTS AND DISCUSSION

For the above set of parameters, the computed numerical results give the evolutions of all the state variables for all the constituents with respect to space and time. Here after the profiles along the specimen of skin are given for some variables for 5 steps of calculations t = 3.2E-4s, 2.4E-3s, 4.8E-3s, 7.2E-3s and 9.6E-3s. Figure 4 gives a zoom of the volumic ratio and the velocity of the ions for 3 steps of calculations t = 3.2E-4s, 2.4E-3s and 4.8E-3s for analysis 1 (Hooke) and analysis 2 (Kelvin-Voigt). In both cases they display a global downward movement of the ions penetrating till the layer with coordinate 13.92E-4 m of the viable epidermis with associated decreasing magnitude of their volumic ratios:

- Analysis 1: 4.875E-45 for the layer-simulating node with coordinate 13.92E-4 m and 3.769E-6 for the upper surface-simulating node with coordinate 15.16E-4 m;

- Analysis 2: 3.551E-44 for the layer-simulating node with coordinate 13.92E-4 m and 3.772E-6 for the upper surface-simulating node with coordinate 15.16E-4 m.

This penetration occurs with a quite high velocity of the ions in spite of the low diffusion coefficient of the skin soft tissues D_i=3.3E-11 $m^2.s^{-1}$. For example for time 4.8E-3s:

- Analysis 1: -3.467E-4 $m.s^{-1}$ for node with coordinate 13.92E-4 m and – 4.361E-4 $m.s^{-1}$ for the upper node with coordinate 15.16E-4 m.
- Analysis 2: -4.030E-4 $m.s^{-1}$ for node with coordinate 13.92E-4 m and – 4.379E-4 $m.s^{-1}$ for the upper node with coordinate 15.16E-4 m.

The velocities tend to increase with respect to time but the curves appear to be quite different. For analysis 2, the velocity varies linearly with the depth which is not at all the case for analysis 1. Figure 5 displays the profiles of the volumic ratio and of the velocity of the fluids. In both analysis, the fluid volumic ratio of the skin surface (stratum corneum) changes almost immediately after application of the chemical and mechanical external loads. The volumic ratio of deeper layers of the skin (viable epidermis and dermis) reacts more slowly. The magnitude of these evolutions are low with values a bit smaller for analysis 2 compared with that of analysis 1 as shown in figure 5 with the overlapping curves. However these evolutions exhibit very different types of movement for the fluids. First the velocity map reveals negative velocities for all nodes of the mesh during the chemical and mechanical loading steps (from 0s to 4.8E-3s). The fluids are flowing slowly from the upper surface layers inward. Then the velocities become positive for all nodes of the mesh during the unloading steps (4.8E-3s to 9.6E-3s). The fluids tend to flow upward in search of a new equilibrium. Again the displayed evolutions depend on the analysis. For example the velocity for node with coordinate 15.04E-4 m is:

- Analysis 1: -6.377E-4 $m.s^{-1}$ for time 2.4E-3s and 1.020E-3 $m.s^{-1}$ for time 9.6E-3s;
- Analysis 2: -6.223E-4 $m.s^{-1}$ for time 2.4E-3s and 9.947E-4 $m.s^{-1}$ for time 9.6E-3s.

The negative displacements of the solids are presented in figure 6. During the chemical and mechanical loading steps (0s to 4.8E-3s), the solids display a consolidation-type behavior all along the specimen of skin-simulating nodes. On the contrary, during the unloading steps (4.8E-3s to 9.6E-3s) the absolute values of the relative displacements become higher and the volume of the specimen increases. Again evolutions are not the same for analysis 1 and for analysis 2. For example the displacement for node with coordinate 15.04E-4 m is:

- Analysis 1: -1.427E-6 m for time 2.4E-3s and -2.035E-7 m for time 9.6E-3s;
- Analysis 2: -1.392E-6 m for time 2.4E-3s and – 1.987E-7 m for time 9.6E-3s.

Both for analysis 1 and for analysis 2, the physics described by the numerical results is coherent with respect to the experimental results available in the literature for indentation experiments on human skin in vivo. When applying chemical and mechanical external loads at the upper outer surface of the skin specimen, it triggers gradients of concentration of ions and gradients of deformations for the solids of the different layers. This starts on one side the penetration of the ions in the upper layers of the stratum corneum because in this case the velocities of the ions are no more equal to zero. On the other side, it starts the downward flows of the different interstitial fluids from the upper surface of the stratum corneum to the deepest layers of the hypodermis linked to non-zero velocities of the fluids of the different layers. At the same time, it also leads to the consolidation-type behavior of the different solids which in its turn will influence the movements of ions and fluids through the hypothesis made with relation (8) on the definition of the Cauchy stress tensor of the total medium. The ions

penetrates the stratum corneum in spite of its structure of dense coating of hard keratinized cells which at the same time opposes a strong tensile strength to the applied mechanical load. The transmitted mechanical load finds then the stratified very souple epithelial of soft living cells of the viable epidermis which tends to answer becoming thinner. The remaining transmitted mechanical load is thus handled by the dermis where the fibrillar network and the amorphous ground substance work together to protect the cells. The consolidation-type behavior of the dermis has a magnitude lower than the one of the viable epidermis. In the last step, the underlying layer, the loose fatty hypodermis, reacts like a rubber-like cushion and consolidate softly under the remaining part of the transmitted mechanical load.

However it is noticeable that analysis 1 and analysis 2 differ with respect to the kinematics of the solids, the fluids and the ions. These not negligible differences give a qualitative insight on the influence of the chosen mechanical laws for the solids of the different layers. In analysis 2, the choice of viscoelastic materials has a smoothing influence on the evolutions of the interstitial fluids flows and ions transport when compared to the same evolutions obtained in analysis 1 where it is considered elastic materials. This induces varying equilibrium of the constantly flowing physiological fluid and coupled varying imbalance in solutes. This can lead to reduction or increase or varying paths for supplies of perfusion, or surface delivery of drugs or creams that can be relevant for chirurgical, clinical and cosmetic treatments.

7 CONCLUSION

In this paper, a tri-phasic stratified skin model has been presented where human skin is composed of four solids, four fluids and ions. The numerical simulation performs reasonably well in describing indentation experiment on human skin in vivo. However the numerical results show differences with respect to the informations on the fluids flows and ions transport when the outside surface of the skin is in contact with a saline solution, depending on the choice between skin seen as elastic or as viscoelastic materials. This skin model offers perspectives for the investigation of the choice of the mechanical behavior of human skin in vivo and its consequences on the delivery routes of physiological fluid and solutes.

REFERENCES

[1] Negrini, D., Moriondo, A. Lymphatic anatomy and biomechanics, *J. Physiol. (*2011) 589, 12, 2927-2934.

[2] Starling, E. H., On the absorption of fluids from the connective tissue spaces, *J. Physiol. Sci.* (1896) **19**:312-326.

[3] Wiig, H. Pathophysiology of tissue fluid accumulation in inflammation, *J. Physiol.* (2011) **589**:2945-2953.

[4] Soltani, M. and Chen, P. Numerical Modeling of Fluid Flow in Solid Tumors. *PLoS ONE 6(6): e20344. doi:10.1371/journal.pone.0020344* (2011).

[5] Levick, J.R. and Michel, C.C. Microvascular fluid exchange and the revised Starling principle. *Cardiovasc Res* (2010) **87**:198–210.

[6] Darling, A.L., Yalavarthy, P.K., Doyley, M.M., Dehghani, H., Pogue, B.W. Interstitial fluid pressure in soft tissue as a result of an externally applied contact pressure, *Phys. Med. Biol.* (2007) **52**:4121–4136.

[7] Zawieja, D.C. Contractile physiology of lymphatics. *Lymphat Res Biol* (2009) **7**:87–96.

[8] Xu, F., Seffen, K., Lu, T. A quasi-linear viscoelastic model for skin tissue. Proceedings of the 3rd IASME/WSIEAS International Conference on Continuum Mechanics (2008).
[9] Flynn, C., Taberner, A.J., Nielsen, P.M.F., Fels, S. Simulating the three-dimensional deformation of in vivo facial skin. *J. of the mechanical behavior of biomedical materials* (2013) **28**:484-494.
[10] Wu, Y., Thalmann, N.M., Thalmann, D. A plastic-visco-elastic model for wrinkles in facial animation and skin aging. *Proceedings of the second Pacific conference on Fundamentals of computer graphics (Pacific Graphics'94)* (1994) 201-213.
[11] P. Jouanna and M-A. Abellan, A generalized approach to heterogeneous media, *Transport in Porous Media* (1996) **25**:351-374.
[12] Abellan, M-A., Zahouani, H., Bergheau J-M. Contribution to the determination of in vivo mechanical characteristics of human skin by indentation test. *Computational and Mathematical Methods in Medicine*, Volume 2013 (2013):Article ID 814025, 11 pages.
[13] Abellan, M-A., Bergheau J-M., Zahouani, H. Modelling the interstitial fluid flow and the mechanical behaviour of intact human skin in vivo. *5th International Conference on Mechanics of Biomaterials and Tissues (ICMoBT)*, 8-12 December, Sitges, Spain, 2013.
[14] Evans, N.D., Oreffo, R.O.C., Healy, E., Thurner, P.J., Man, Y.H. Epithelial mechanobiology, skin wound healing, and the stem cell niche. *J. of the mechanical behavior of biomedical materials* (2013) **28**:397-409.

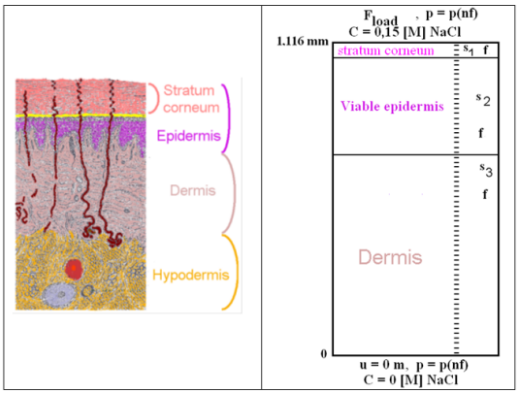

Figure 1: Schematic view of the cross-section of human skin (left) and of the skin specimen (right) showing the finite difference mesh and the boundary conditions

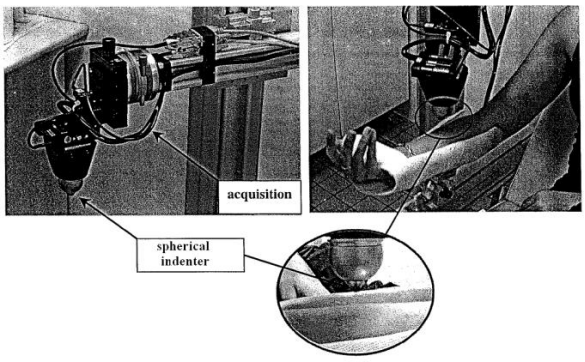

Figure 2: Experimental set-up of the LTDS-indentation device

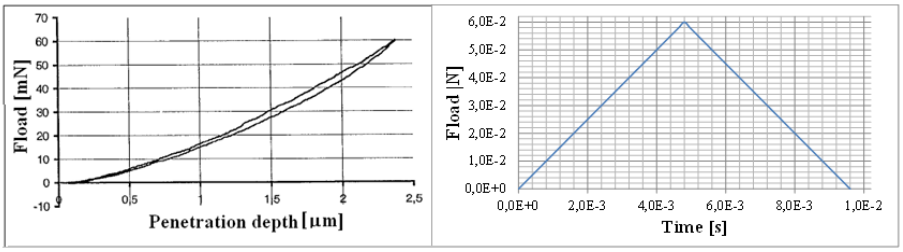

Figure 3: (left) Recorded curve for a loading-unloading indentation test on the volar forearm of an adult. (right) Applied mechanical load versus time for the loading steps of the numerical simulations

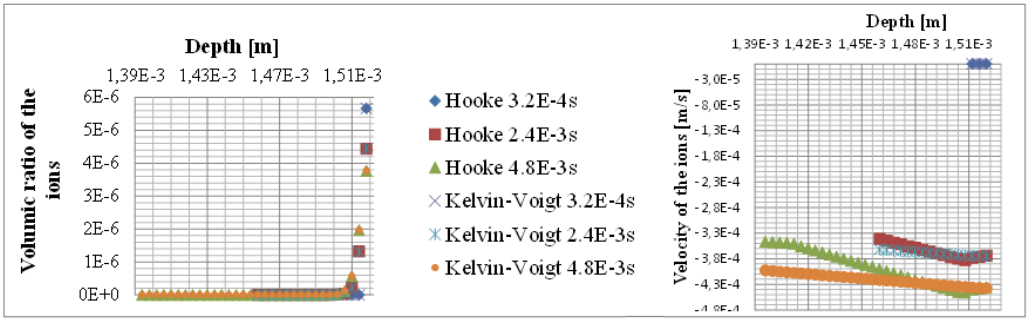

Figure 4: Volumic ratio (left) and velocity (right) of the ions

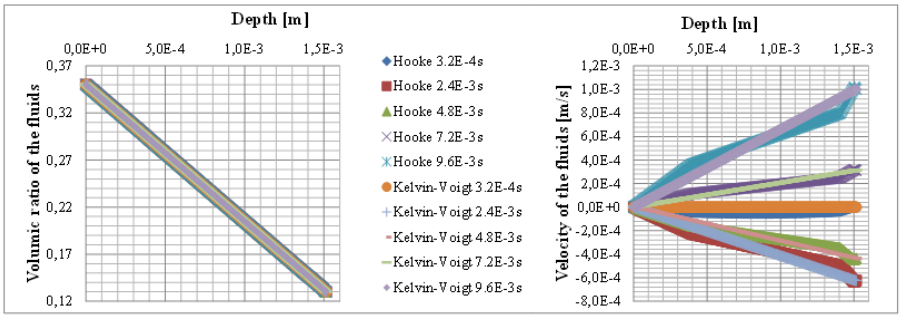

Figure 5: Volumic ratios (left) and velocities (right) of the fluids

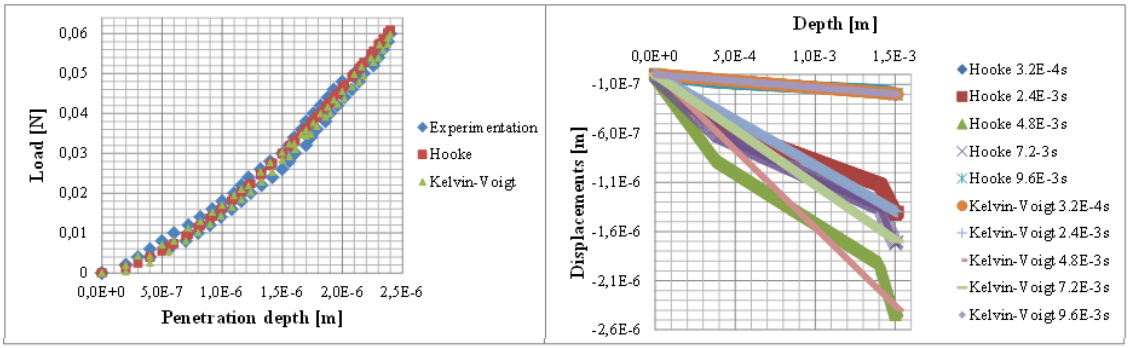

Figure 6: (left) Comparison between numerical and experimental displacement curves (right) Displacements of the solids